JNS

LABORATORY INVESTIGATION

J Neurosurg 136:1726–1737, 2022

Vortex formation and associated aneurysmogenic transverse rotational shear stress near the apex of wide-angle cerebral bifurcations

Adel M. Malek, MD, PhD, James E. Hippelheuser, MS, and Alexandra Lauric, PhD

Department of Neurosurgery, Tufts Medical Center and Tufts University School of Medicine, Boston, Massachusetts

OBJECTIVE Aneurysm formation preferentially occurs at the site of wide-angle cerebral arterial bifurcations, which were recently shown to have a high longitudinal positive wall shear stress (WSS) gradient that promotes aneurysm formation. The authors sought to explore the other components of the hemodynamic environment that are altered with increasing bifurcation angle in the apical region and the effects of these components on WSS patterns on the vessel wall that may modulate aneurysm genesis and progression.

METHODS Parametric models of symmetrical and asymmetrical bifurcations were created with increasing bifurcation angles (45°–240°), and 3D rotational angiography models of 13 middle cerebral artery (MCA) bifurcations (7 aneurysmal, 6 controls) were analyzed using computational fluid dynamics. For aneurysmal bifurcations, the aneurysm was digitally removed to uncover hemodynamics at the apex. WSS vectors along cross-sectional planes distal to the bifurcation apex were decomposed as orthogonal projections to the cut plane into longitudinal and transverse (tangential to the cross-sectional plane) components. Transverse rotational WSS (TRWSS) and TRWSS gradients (TRWSSGs) were sampled and evaluated at the apex and immediately distal from the apex.

RESULTS In parametric models, increased bifurcation angle was associated with transverse flow vortex formation with emergence of an associated apical high TRWSS with highly aneurysmogenic positive TRWSSGs. While TRWSS decayed rapidly away from the apex in narrow-angle bifurcations, it remained greatly elevated for many radii downstream in aneurysm-prone wider bifurcations. In asymmetrical bifurcations, TRWSS was higher on the aneurysm-prone daughter vessel associated with the wider angle. Patient-derived models with aneurysmal bifurcations had wider angles (149.33° ± 12.56° vs 98.17° ± 8.67°, $p < 0.001$), with significantly higher maximum TRWSS (1.37 ± 0.67 vs 0.48 ± 0.23 Pa, $p = 0.01$) and TRWSSG (1.78 ± 0.92 vs 0.76 ± 0.50 Pa/mm, $p = 0.03$) compared to control nonaneurysmal bifurcations.

CONCLUSIONS Wider vascular bifurcations are associated with a novel and to the authors' knowledge previously undescribed transverse component rotational wall shear stress associated with a positive (aneurysmogenic) spatial gradient. The resulting hemodynamic insult, demonstrated in both parametric models and patient-based anatomy, is noted to decay rapidly away from the protection of the medial pad in healthy narrow-angle bifurcations but remain elevated distally downstream of wide-angle aneurysm-prone bifurcations. This TRWSS serves as a new contribution to the hemodynamic environment favoring aneurysm formation and progression at wide cerebral bifurcations and may have clinical implications favoring interventions that reduce bifurcation angle.

https://thejns.org/doi/abs/10.3171/2021.6.JNS204385

KEYWORDS intracranial aneurysms; bifurcation apex; wall shear stress; flow recirculation; vascular disorders

The anatomically localized pattern for cerebral aneurysm formation at arterial bifurcations strongly implicates hemodynamic forces in this pathological process.[1] In particular, wall shear stress (WSS), the frictional force exerted by blood flow on the vessel wall, has been determined to impact the mechanics of the arterial wall and to be a critical mediator of gene expression regulation via endothelial mechanoreceptors.[2] Studies have shown that altering local fluid mechanics by surgically creating de novo branching points resulted in distinct patterns of vessel wall remodeling, disrupted endothelium, and presence of inflammatory cells. These are all changes that closely resemble the initiation of intracranial aneurysms.[3–5] Research suggests that the flow pattern charac-

ABBREVIATIONS CFD = computational fluid dynamics; MCA = middle cerebral artery; TRWSS = transverse rotational WSS; TRWSSG = TRWSS gradient; TRWSSGP = product of high TRWSS and high positive TRWSSG; WSS = wall shear stress; WSSG = WSS gradient.

SUBMITTED December 20, 2020. **ACCEPTED** June 15, 2021.

INCLUDE WHEN CITING Published online October 29, 2021; DOI: 10.3171/2021.6.JNS204385.

©AANS 2022, except where prohibited by US copyright law

Brought to you by Tufts University | Unauthenticated | Downloaded 11/04/25 02:24 PM UTC

teristic of vulnerable vascular geometries (such as cerebral bifurcations), which has been identified as disturbed laminar shear stress,[6] is the likely agent promoting endothelium alterations. Of importance was the discovery of the dichotomy between hemodynamic conditions of quiescence when WSS is associated with a negative spatial WSSG (gradient is in opposite direction to WSS) versus those favoring vessel wall degradation and aneurysm formation where WSS is associated with a positive spatial WSSG.[3–6]

Predisposing bifurcation geometry was previously studied by our group. On a large cohort of control and aneurysmal bifurcations, it was shown that basilar and middle cerebral aneurysmal bifurcations were significantly wider than the control bifurcations.[7,8] This widening induced an expansion of the accelerating region of high WSS and WSS gradients (WSSGs) migrating distally from the bifurcation apex.[8] It was proposed that in narrow bifurcations the impingement area was positioned within the physiological bounds of a protective medial pad which provides strength and stiffness to the region.[9,10] Wide-angle bifurcations were shown to be characterized by induction of an aneurysmogenic highly positive WSS gradient in the longitudinal direction.[11]

However, in many cases aneurysms do not occur at the apex, but rather originate off of one of the daughter vessels, especially at wider angles.[7] The purpose of this study was to explore the effect of the widening of the bifurcation angle on the hemodynamic environment downstream from the bifurcation apex. In order to quantify the behavior of the flow in regions of secondary circulation characteristics of arterial bifurcations, we represented WSS vectors as linear combinations of the longitudinal WSS[11] (in the direction of the vessel centerline) and transverse rotational WSS (TRWSS; in planes perpendicular to the vessel axis). In the current study we identified a new significant TRWSS which begins near the impingement zone and extends significantly toward the daughter vessels, especially at the wider branching angles encountered in aneurysmal bifurcations.

Methods

Parametric Models

To evaluate the effect of increasing bifurcation angle on the TRWSS in the region of the bifurcation apex, parametric models of the middle cerebral artery (MCA) bifurcations were constructed using SolidWorks. Consistent with previous nomenclature[7,12] (Fig. 1A), the daughter vessel with the larger caliber is identified with numeral 1 and its corresponding angle Φ_1, while the smaller daughter is associated with angle Φ_2.

The first set of parametric models were created with a straight parent vessel having a length of 15 mm and a radius of 1.3 mm. Symmetrical daughter vessels (length 10 mm, radius 1.032 mm) were joined to the mother vessel using a joining sphere with a concentric radius of 1.3 mm. The combination of the radii for the mother and daughter vessels followed the vascular optimality principle.[13] Five bifurcation models were created with total bifurcation angles ($\Phi_1 + \Phi_2$) of 45°, 60°, 120°, 180°, and 240° (Fig. 1B).

A second set of asymmetrical parametric models was created, starting from the $\Phi_1 = \Phi_2 = 30°$ symmetric model and increasing only one of the daughter angles by increments of 30° to $\Phi_2 = 60°$ and 90°, yielding total bifurcation angles of 90° and 120° (Fig. 1C).

Patient Selection and Demographics

Consecutive high-resolution 3D angiographic data of recently treated patients with MCA aneurysms, as well as normal controls, were analyzed for this study, including 7 aneurysmal MCAs (mean patient age 59.4 years, 5 females) and 6 nonaneurysmal MCAs (mean patient age 62.2 years, 2 females). Patients were selected randomly from a prospectively maintained database of MCA aneurysms and healthy controls as previously described.[7]

Cerebral Angiography and Data Processing

3D cerebral angiograms were obtained from Siemens Artis biplane systems and reconstructed using the Leonardo clinical software packages to yield a 3D volume (Fig. 1D). Volumetric data sets, including aneurysm and parent vessel, were analyzed in Amira version 5.4 (FEI) for segmentation in 3D space (Fig. 1E).

Patient-Derived Models

Following vessel segmentation, aneurysms were digitally removed by local Laplacian smoothing as previously described,[11] and parent vessels were reconstructed in MeshLab version 1.3.1 (ISTI-CNR) (Fig. 1E). The MCA segment proximal to the site of the aneurysm was kept sufficiently long to enable the laminar flow to become fully developed and avoid entrance effects.

Computational Fluid Dynamics

The resulting surfaces were used to create polyhedral computational meshes with boundary layer enhancement using Star-CCM+ (CD-Adapco). The resulting mesh was of sufficient density to ensure grid independence. Computational fluid dynamics (CFD) simulations were performed using Ansys Fluent 14.0 (Ansys), by modeling laminar transient flow with a Carreau non-Newtonian profile to better approximate the viscosity and flow of blood.[14] For each model, the velocity magnitude was scaled to ensure an ideal parent vessel WSS of approximately 1.5 Pa in the proximity of the aneurysm.[15] Pulsatile flow was applied at the inlet for three complete cardiac cycles to allow flow to develop adequately, and the third cycle was used for analysis. Each cycle period was T = 1 second and had a time step of t = 0.002 seconds with the peak systole at t = 0.16 seconds. At the outlets, gauge pressure was set to 0 Pa.[16]

To simulate a change in flow resistance within the daughter vessels for one asymmetrical model ($\Phi_1 = 30°$/$\Phi_2 = 90°$), CFD simulations were repeated using nonzero outlet gauge pressure. First, an outlet gauge pressure of 25 Pa was set at the daughter forming $\Phi_2 = 90°$ with the parent vessel, while the outlet gauge pressure at the daughter forming a $\Phi_1 = 30°$ angle was kept at zero. Second, the outlet gauge pressure at the daughter forming a $\Phi_2 = 90°$ angle daughter was increased from 25 to 35 Pa, while keeping zero gauge pressure at the $\Phi_1 = 30°$ daughter outlet.

Brought to you by Tufts University | Unauthenticated | Downloaded 11/04/25 02:24 PM UTC

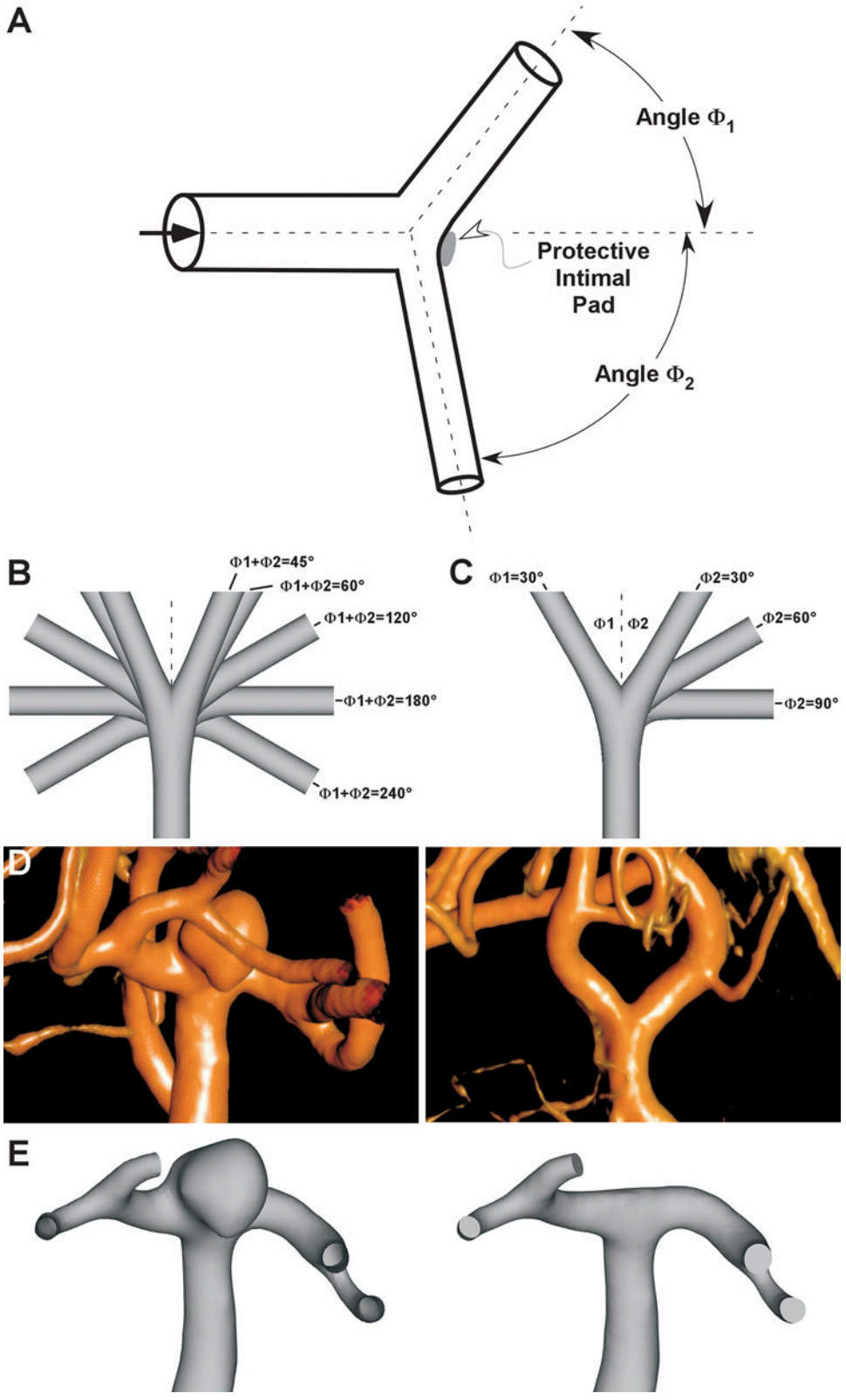


FIG. 1. A: Nomenclature of cerebral bifurcation geometry showing protective intimal pad with angle Φ_1 formed by the larger-caliber daughter vessel and Φ_2 by the smaller-caliber vessel. **B:** Idealized parametric symmetric bifurcation models ($\Phi_1 = \Phi_2$, and total bifurcation angles $\Phi_1 + \Phi_2 = 45°$, 60°, 120°, 180,° and 240°). **C:** Asymmetrical parametric models (fixed $\Phi_1 = 30°$ angle, and varying $\Phi_2 = 30°$, 60°, or 90°). **D:** Volumetric rendering of a patient-based 3D rotational angiographic data set showing an MCA aneurysm (*left*) and a control nonaneurysmal MCA bifurcation (*right*). **E:** Segmentation of the aneurysmal MCA bifurcation volumetric data set before (*left*) and after (*right*) aneurysm digital removal using Laplacian smoothing. Figure is available in color online only.

Brought to you by Tufts University | Unauthenticated | Downloaded 11/04/25 02:24 PM UTC

Postprocessing analysis was performed using EnSight 10.1 (Ansys). For each model, WSS was evaluated along cross-sectional cuts orthogonal to the daughter vessels starting at the apex and moving distally at equal increments. For parametric data, cross-sectional planes are sampled at the apex and then in increments of 1 mm. For patient-derived data, cross-sectional planes are sampled in increments of one radius distance, with the first plane placed at one radius distance from the apex. Cutting plane coordinates were evaluated using the Vascular Modeling Toolkit.[17] WSS vectors along these cross-sectional planes were decomposed 1) as orthogonal projections onto the cut plane (transverse WSS, tangent on the cross-sectional plane) and 2) in the direction of the normal to the cut plane (longitudinal WSS[11]). Analysis of the TRWSS and the TRWSS gradient (TRWSSG) was used to quantify flow recirculation in the impingement area and the outward fill of the daughter vessels (Fig. 2A).

Results

Wide Bifurcation Angle, Vortex Formation, and Rotational WSS

Increasing the bifurcation angle in parametric symmetric bifurcation results in increasing flow stagnation at the apex and outward flow recirculation into the daughter vessels (Fig. 3). In orthogonal, cross-sectional planes on daughter vessels, flow recirculation is stronger and better defined closer to the bifurcation, dissipating distally (Fig. 3A). Wider bifurcations are characterized by stronger and more persistent recirculation as well as formation of flow vortices (Fig. 3) with generation of transverse velocity fields not seen in narrow counterparts.

In symmetric models, the TRWSS component is stronger closer to the bifurcation apex and decreases distally toward zero (Fig. 2B). This fading phenomenon is slower at wider bifurcation angles (Fig. 4). The magnitude of TRWSS also increases with angle size, suggesting a more vigorous recirculation movement in wider bifurcations (Fig. 4B). Moreover, wider angles result in a widening of the region of flow separation and vortex formation (from zero TRWSS to the TRWSS peak magnitude). In addition, these are regions characterized by high positive TRWSSG. Thus, the section of the daughter vessel subjected to both high TRWSS and high positive TRWSSG widens with an increase in the bifurcation angle, as illustrated by the product of these variables (TRWSSGP), with a positive value of the latter associated with aneurysmal degenerative change and a negative value being protective, respectively (Fig. 4B).

In asymmetrical models, the TRWSS component is stronger on the daughter vessel corresponding to the larger angle (Fig. 5A, Videos 1 and 2).

VIDEO 1. Side view of an asymmetrical bifurcation having 90° on the left branch and 30° on the right branch undergoing pulsatile flow simulation using CFD with tangential rotational WSS vectors color-coded with shear stress magnitude (blue = 0 and red = 1.5 Pa). Note the much higher TRWSS in the wide-angle left branch compared to the narrow-angle right branch. Copyright Adel M. Malek. Published with permission. Click here to view.

VIDEO 2. View of the same simulation and geometry imaged from the top view looking down (same TRWSS maginitude scale). Copyright Adel M. Malek. Published with permission. Click here to view.

The magnitude of TRWSS converges faster on the narrower side (Fig. 5B), with a slower outward fill on the wider side of the bifurcation (Fig. 5C). Similarly to the symmetric models, increasing the bifurcation angle in the asymmetrical models results in higher TRWSS magnitude, widening of the region of flow separation, high positive TRWSSG (Fig. 5C), and an extension of the region exposed to deleterious positive TRWSSGP.

Patient-Derived Models

Consistent with previously reported results,[7] aneurysmal MCA bifurcations had significantly larger total bifurcation angles ($\Phi_1 + \Phi_2 = 149.33° \pm 12.56°$ vs $98.17° \pm 8.67°$, $p < 0.001$) and significantly larger angles formed between the parent vessel and the smaller daughter vessel (Φ_2, $89.46° \pm 15.79°$ vs $49.07° \pm 4.32°$, $p < 0.001$) (Fig. 6A), compared to nonaneurysmal MCA bifurcations (Fig. 6B). There was no statistical difference between the angle formed by the parent vessel and the larger daughter vessel (Φ_1, $59.87° \pm 5.83°$ vs $49.10° \pm 6.30°$, $p = 0.24$). In addition, for 5 out of 6 aneurysmal MCAs, Φ_1 was much smaller than Φ_2, but this trend was not noticed in the nonaneurysmal bifurcations. The aneurysms originated off of the smaller daughter vessel in 4 cases, in which Φ_1 was much smaller than Φ_2. The aneurysms originated at the apex in two cases, in which the two angles were very close to being equal.

Time average TRWSS and maximum TRWSS were evaluated distally from the bifurcations on both daughter vessels (Fig. 6C). As evident in Fig. 6C, maximum TRWSS on the larger daughter vessel (corresponding to Φ_1) was significantly higher in aneurysmal bifurcations than in control bifurcations (1.37 ± 0.67 vs 0.48 ± 0.23 Pa, $p = 0.01$) (Table 1, Fig. 6D). Similarly, maximum TRWSSG on the larger daughter vessel was significantly higher for bifurcations harboring aneurysms than for controls (1.78 ± 0.92 vs 0.76 ± 0.50 Pa/mm, $p = 0.03$) (Fig. 6).

It should be noted that, in contrast to idealized morphologies which allow for the isolation of TRWSS in controlled hemodynamic environments, patient morphology presents a multitude of morphological combinations, including varying vessel diameters and nonzero inclination angles (defined as the angle between the parent vessel and the plane formed by the daughter vessels[7]). These morphological variations, which are beyond the scope of this study, likely account for the small differences between parametric and patient-derived TRWSS results.

Effect of Simulated Resistance in Daughter Vessels on Transverse WSS

We have previously shown that whereas nonaneurysmal MCA bifurcations follow the vascular optimality principle,[13] MCA bifurcations harboring aneurysms do not behave according to optimality laws decreeing constant WSS in parent and daughter vessels.[7] Because all parametric models presented here follow the optimality principle, we attempted to simulate flow resistance in daughter vessels by using nonzero outlet gauge pressure in order to examine the sensitivity of TRWSS to morphological fac-

Brought to you by Tufts University | Unauthenticated | Downloaded 11/04/25 02:24 PM UTC

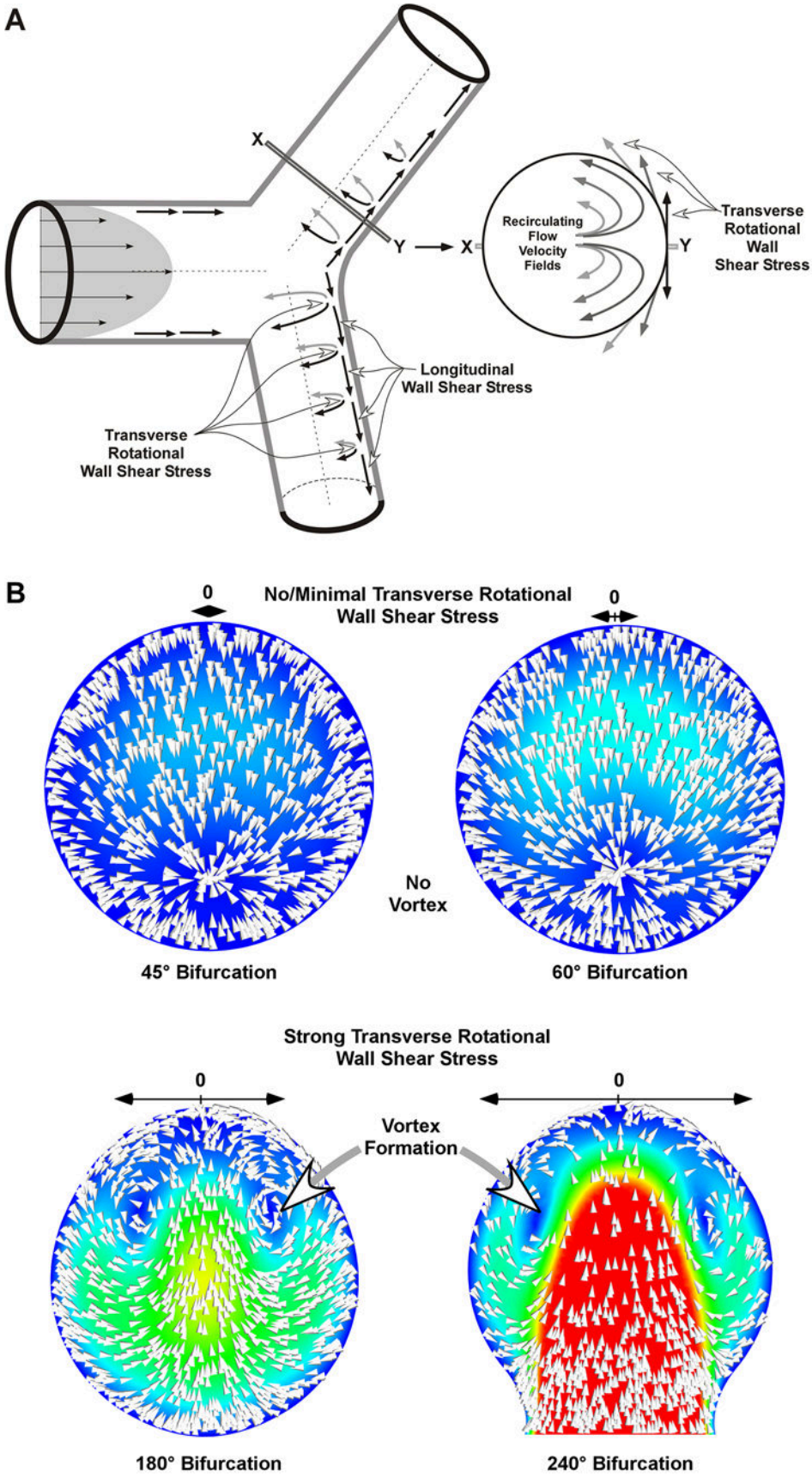


FIG. 2. A: Perspective schematic illustration of the longitudinal and transverse rotational wall shear stress (TRWSS) components (*left*) with cross-section at X-Y illustrating flow recirculation and associated TRWSS. **B:** Magnified view of cross-sectional orthogonal planes downstream at 2 radii (*orange cut*) in bifurcation angles from 45° to 60°, 180°, and 240°; note the rotational vortex formation at 180° and 240° with the resulting increasing tangential direction of flow velocity vectors resulting in strong TRWSS in contrast to mostly nontangential direction at 45° and 60°. Figure is available in color online only.

Brought to you by Tufts University | Unauthenticated | Downloaded 11/04/25 02:24 PM UTC

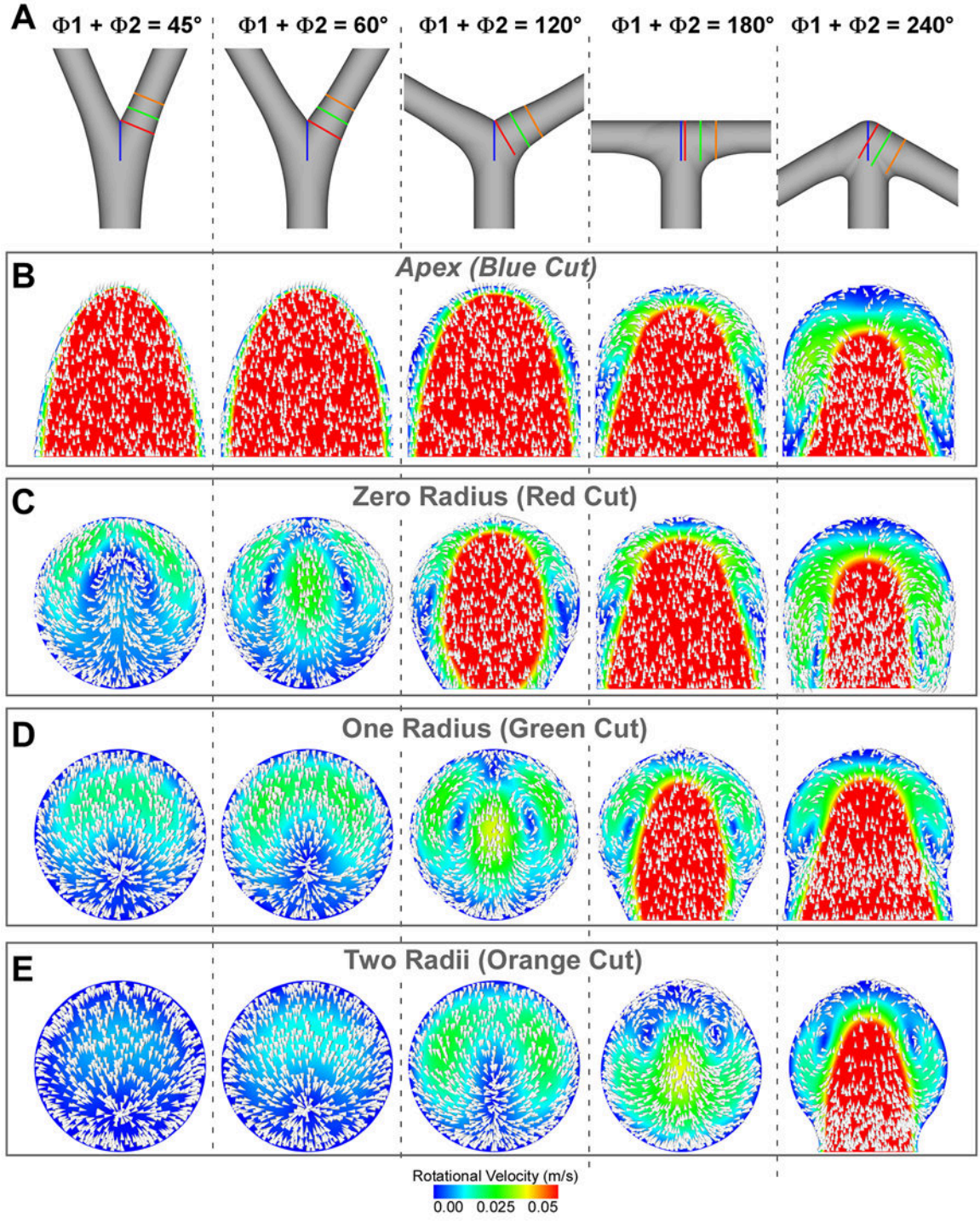


FIG. 3. Cross-sectional velocity profiles, in a plane orthogonal to the daughter vessel, of parametric symmetric bifurcations (Φ_1 + Φ_2 = 45° to 240°) (**A**) starting at the apex (**B**) and moving downstream the daughter vessel from zero (**C**) to 1-radius (**D**) and 2-radii (**E**) distance. The corresponding overlaid transverse flow velocity component indicates direction of flow vectors and development of flow vortices that increase in magnitude and propagate deeper downstream from the apex with increasing total bifurcation angle (Φ_1 + Φ_2). Figure is available in color online only.

tors which may impact the optimality principle and induce vessel resistance, such as change in daughter diameter, vessel curvature, and total length of the daughter segment (Fig. 7A). As shown in Fig. 7B, changing the outlet gauge pressure at Φ_2 = 90° from 0 to 25 Pa translated to a 40% velocity decrease in the large-angle daughter vessel and to a 38% velocity increase in the smaller-angle daughter vessel (Φ_1 = 30°). TRWSS proved sensitive to change in

Brought to you by Tufts University | Unauthenticated | Downloaded 11/04/25 02:24 PM UTC

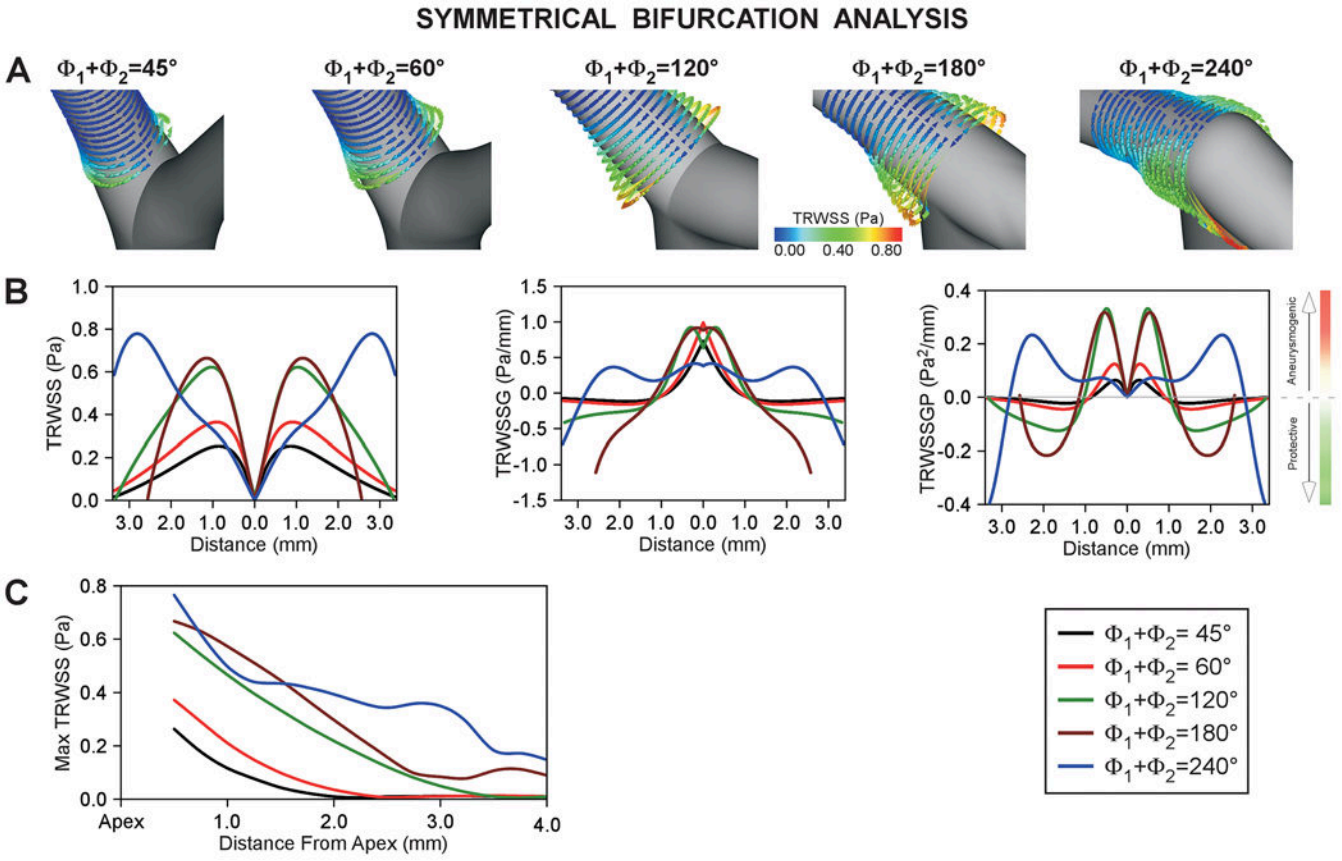


FIG. 4. Analysis of transverse rotational wall shear stress (WSS) on symmetric parametric models. **A:** TRWSS vectors on plane cuts orthogonal on the daughter vessel branch, starting near the 0-mm radius and moving distally in 0.25-mm increments, color-coded for shear stress magnitude. **B:** Plots of the TRWSS (*left*) and its spatial gradient, TRWSSG (*middle*), sampled at the first cut plane to the bifurcation, starting from counterclockwise 3.25 mm to clockwise 3.25 mm from the apex line (12 o'clock top), and their product, the transverse rotational wall shear stress gradient product (TRWSSGP) (*right*); positive TRWSSGP values are aneurysmogenic while negative values are protective. Note increasing proportion and spatial extent of positive aneurysmogenic product values at larger angles. **C:** Maximum TRWSS magnitude at increasing distances downstream into the daughter branch from the apex, showing rapid decay at small bifurcation angles with persistently elevated values at larger 180° and 240° bifurcation angles. Figure is available in color online only.

flow resistance compared with the controlled model (zero gauge pressure at both outlets). When outlet gauge pressure of 25 Pa was applied at the large-angle daughter vessel (simulating increased flow resistance), TRWSS in the 90° branch decreased by 22%, while TRWSS in the small-angle daughter increased by only 2.6% compared to the control (Fig. 7B). Increasing outlet gauge pressure to 35 Pa at the large-angle daughter resulted in a further decrease of TRWWS in the 90° branch (18%), resulting in a 36.5% total TRWSS decrease compared to the control model. This modeling simulates conditions in which the daughter vessel with a smaller vessel diameter (increased flow resistance) is associated with a larger angle, whereas the daughter vessel with the larger diameter is associated with a smaller angle. This particular bifurcation morphology was previously associated with aneurysmal presence,[7,8] and it is indicative of the aneurysmal sample used in this study.

Discussion

Cerebral arterial bifurcations represent preferred sites for aneurysm formation, especially when associated with variations in divider geometry. Arterial bifurcations are designed to maintain WSS at optimum levels, thereby minimizing energy expenditure.[18,19] The underlying mechanisms responsible for controlling the dynamic vasoregulatory process may be impaired at aneurysm sites. It was shown that alterations in bifurcation geometry, namely angle size and vessel radius, create hemodynamic conditions that can predispose the bifurcation to the development and progression of intracranial aneurysms.[20,21] In a large cohort of aneurysmal bifurcations (MCA[7] and basilar artery[8]), we have previously shown that larger bifurcation angle was associated with aneurysmal presence. Previous work also showed that the basilar artery widens with age, starting at maturity, more so in female patients, suggesting a natural remodeling of the bifurcation morphology, that may induce local hemodynamic changes predisposing the apical region to aneurysm formation.[8]

Hemodynamic evaluation of those regions showed that larger bifurcation angles were associated with a widening of the impingement area,[8,11] potentially beyond the protec-

Brought to you by Tufts University | Unauthenticated | Downloaded 11/04/25 02:24 PM UTC

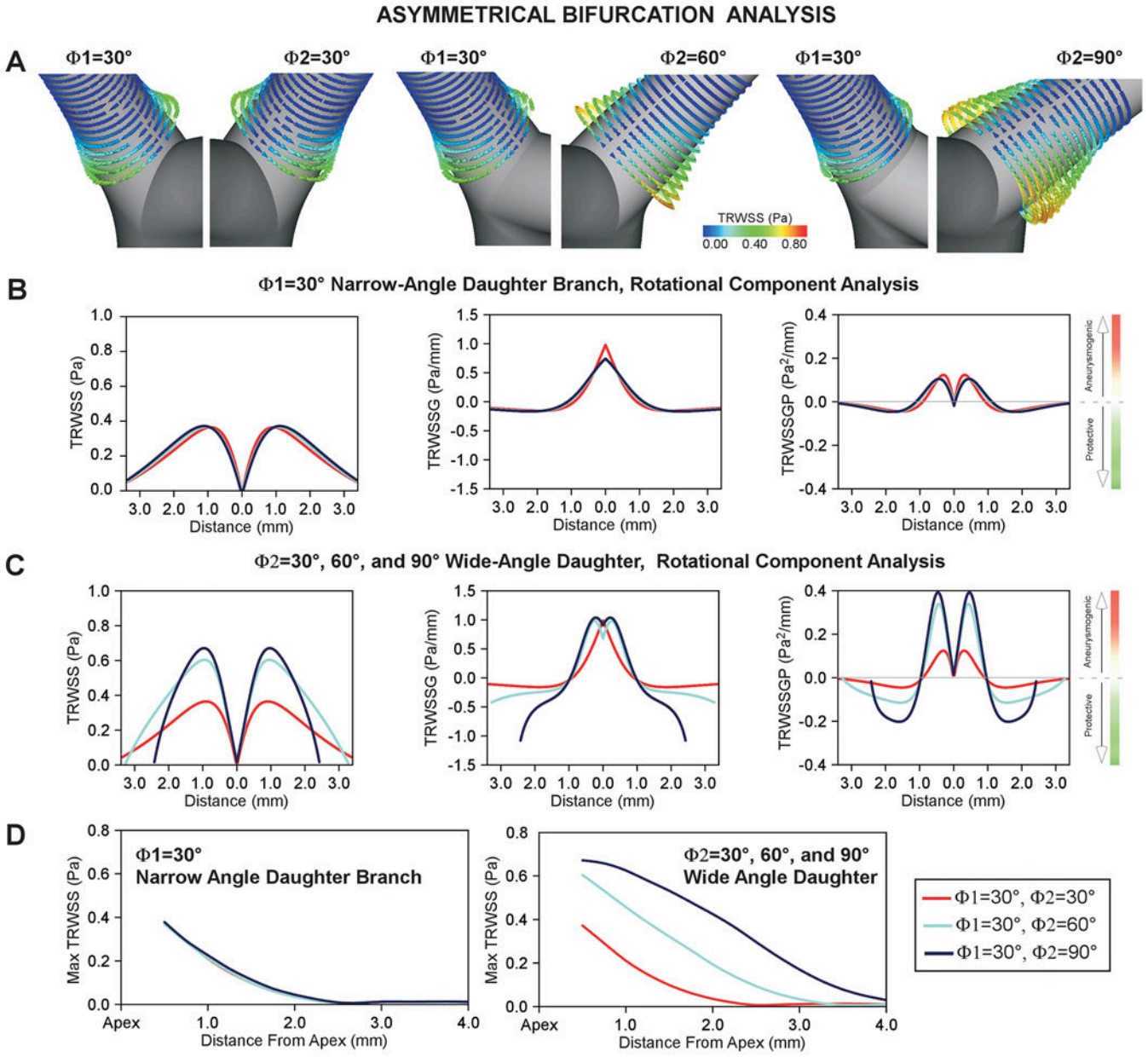


FIG. 5. Analysis of transverse rotational wall shear stress (WSS) on asymmetrical parametric models, with Φ_1 held at 30° with increasing Φ_2 from 30° to 90°. **A:** TRWSS vectors on plane cuts orthogonal to the parent vessel, starting at the apex and moving distally in 0.25-mm increments. Vectors on the right of each figure correspond to branches with increasing angles (Φ_2 = 30°, 60°, and 90°). **B:** Plots of the TRWSS, TRWSSG, and their product TRWSSGP sampled on the first cut plane for the Φ_1 held at 30° show no significant change with increasing angle of the other daughter vessel branch. **C:** Plot of the same variable on the daughter branch with increasing angles (Φ_2 = 30°, 60°, and 90°) reveals development of higher aneurysmogenic TRWSSGP with increasing angles on the wider branch with the angle increase. **D:** Maximum TRWSS magnitude at increasing distances downstream into the daughter vessel branches shows rapid decline on the 30° narrow angle branch (*left*) with increasing TRWSS values at greater downstream distances from the apex with increasing angles on the wide-angle daughter vessel branch (*right*). Figure is available in color online only.

tive apical collagen band that provides strength and stiffness to the bifurcation apex.[9] This finding is particularly significant as we have previously shown that 68% of MCA aneurysms originated off the daughter vessel branches, off-center from the bifurcation apex.[7]

Whereas previously reported studies have focused on the longitudinal aspect of the bifurcation apex,[11] here we identified and characterized a novel transverse rotational component of the WSS (TRWSS) that can be used to evaluate the hemodynamic conditions within the daughter vessel branches just distal to the apex, because the flow forms vortices when it is separated at wide-angle bifurcations and diverted downstream into the daughter arteries. Importantly, this transverse wall shear component and its positive spatial gradient constitute an aneurysmogenic hemodynamic condition as opposed to a protective nega-

Brought to you by Tufts University | Unauthenticated | Downloaded 11/04/25 02:24 PM UTC

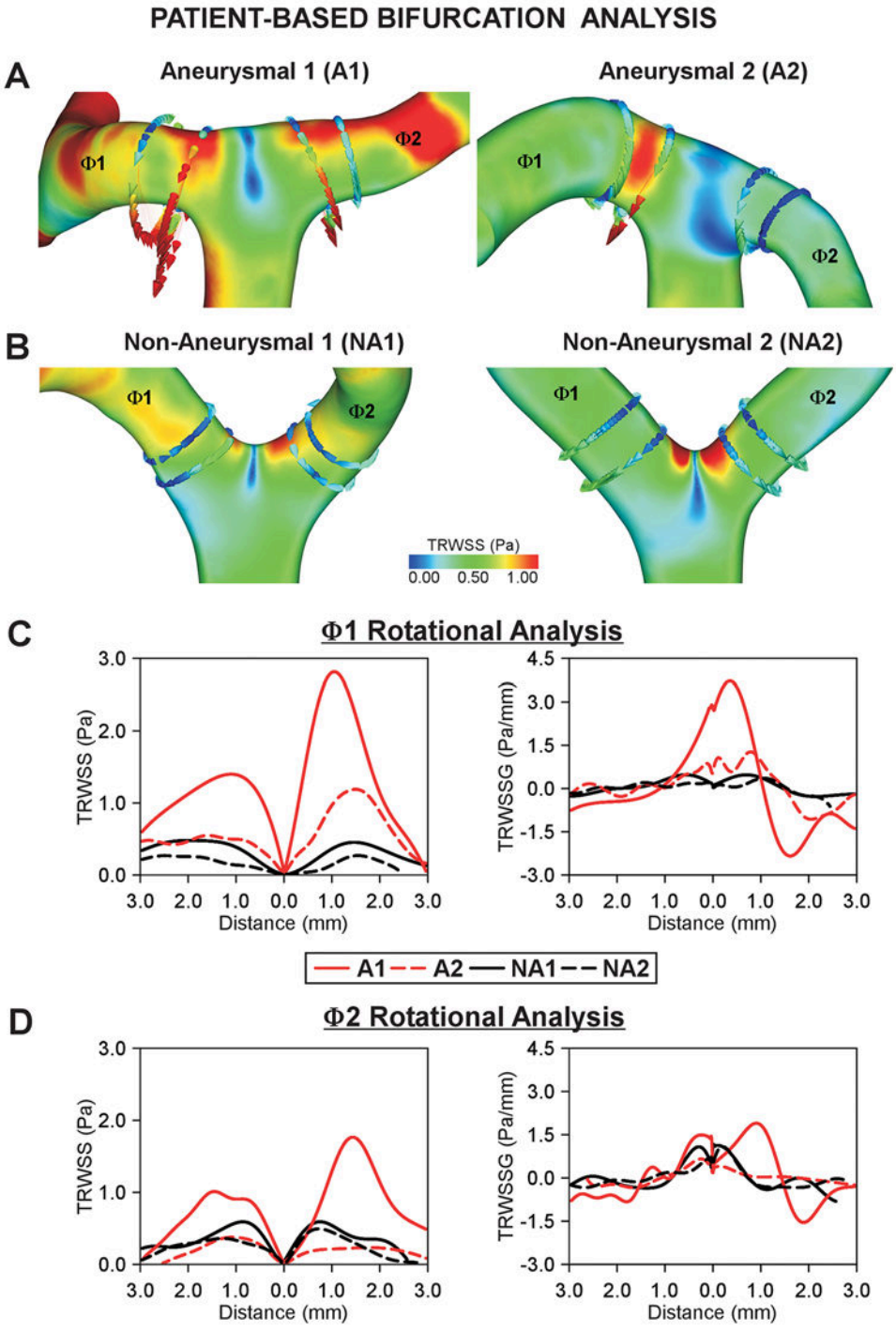


FIG. 6. Analysis of transverse rotational wall shear stress (WSS) on patient-derived data. **A:** TRWSS on aneurysmal bifurcations with high shear magnitude–colored tangential vectors in both aneurysmal wide-angle bifurcations persisting beyond the apex (more pronounced in A1 than A2). **B:** TRWSS on nonaneurysmal bifurcations; note lower magnitude of rapidly declining tangential shear vectors within a short distance from the apex. **C:** Plots of TRWSS and TRWSSG at the first cut plane on the Φ_1 branch (left daughter branch). **D:** Plots of TRWSS and TRWSSG at the first cut plane on the Φ_2 branch (right daughter vessel branch). Note similar pattern seen in the parametric models within biological variability. Figure is available in color online only.

tive spatial shear gradient.[3–6,11] Indeed, analysis of TRWSS on parametric models showed higher TRWSS magnitude closer to the bifurcation apex and a fading TRWSS component distal from the point of flow separation in all models. A wider bifurcation angle is associated with higher TRWSS and slower flow convergence. In asymmetrical models, TRWSS is much higher on the side with the larger angle and increases with the increase in the branch an-

Brought to you by Tufts University | Unauthenticated | Downloaded 11/04/25 02:24 PM UTC

TABLE 1. Comparison of TRWSS in aneurysmal and normal MCA bifurcations

Transverse WSS Parameter	Bifurcation		p Value
	Aneurysmal	Normal Nonaneurysmal	
Branch Φ_1			
Max TRWSS (Pa)	1.37 ± 0.67	0.48 ± 0.23	**0.01**
Max TRWSSG (Pa/mm)	1.78 ± 0.92	0.76 ± 0.50	**0.03**
Max TRWSSGP (Pa^2/mm)	1.74 ± 2.11	0.26 ± 0.30	0.12
Branch Φ_2			
Max TRWSS (Pa)	0.85 ± 0.78	0.49 ± 0.20	0.30
Max TRWSSG (Pa/mm)	1.24 ± 0.82	1.16 ± 0.54	0.86
Max TRWSSGP (Pa^2/mm)	0.97 ± 1.31	0.39 ± 0.35	0.31

Statistical analysis of TRWSS, its spatial gradient (TRWSSG), and their product (TRWSSGP) in patient-based models. Branch Φ_1 is the larger daughter vessel. Branch Φ_2 is the daughter vessel associated with a smaller vessel diameter. Values are shown as mean ± SD unless otherwise indicated. Boldface type indicates statistically significant p value < 0.05.

gle. This finding correlates with our previous reports on MCA bifurcations showing that aneurysms more often originate off the daughter vessel associated with a wider angle.[7] We hypothesize that vascular bifurcations may not be equipped to sustain the hemodynamic stress associated with this aneurysmogenic positive gradient transverse WSS component in regions distal to the apical pad.

In patient-derived data, TRWSS and its spatial gradient TRWSSG were significantly higher in patient-derived aneurysmal bifurcations than in controls. However, in contrast to parametric models, there was not a clear correlation between high TRWSS and the daughter vessel forming the larger angle. We hypothesized that this lack of correlation was the effect of variations in daughter diameters. Whereas parametric models follow the vascular optimality principle,[13] all aneurysmal bifurcations in this study (as most aneurysmal bifurcations[10,12]) disobey this principle.[13] It should be noted that the purpose of our hemodynamic analysis in patient models was to evaluate a representative selection of random aneurysmal and nonaneurysmal bifurcations for emergence of TRWSS patterns. Because nonoptimal bifurcation conditions imply

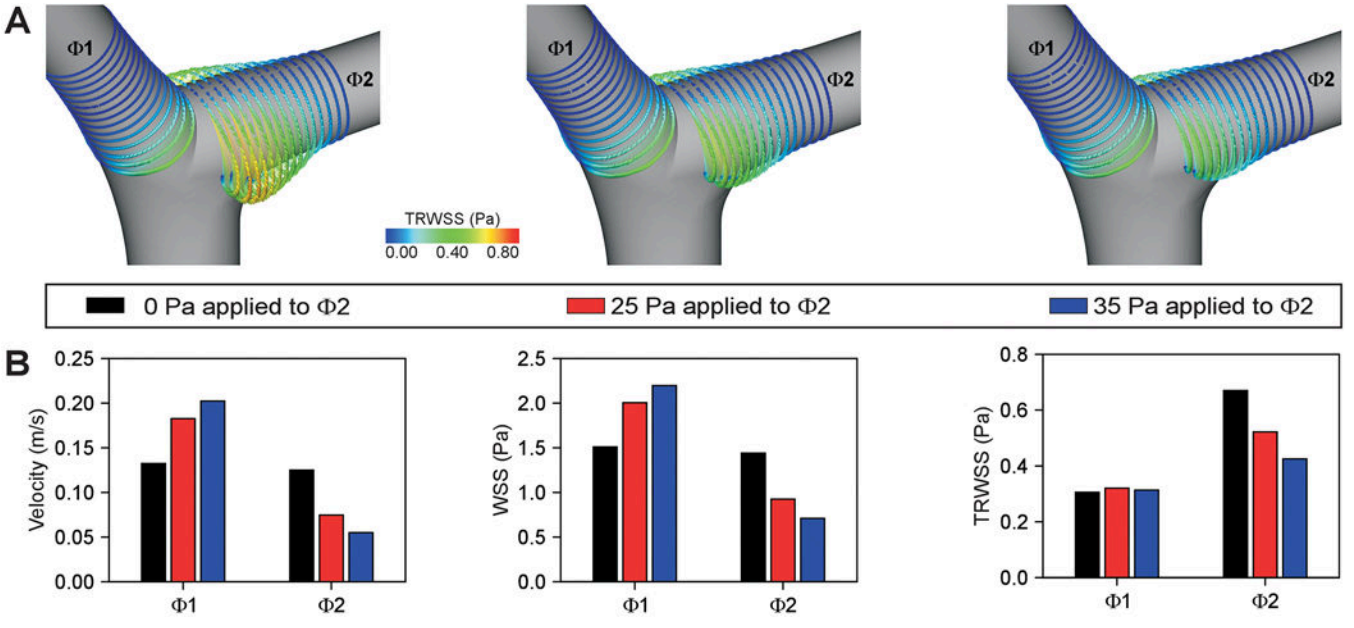


FIG. 7. Simulation of the effect of downstream flow resistance within the daughter vessels for one asymmetrical parametric model (Φ_1 = 30°, Φ_2 = 90°) in an attempt to assess the effect of relative flow reduction in wide-angle 90° branch 2 performed by increasing the gauge pressure at the daughter vessel outlet. **A:** Original model with an outlet gauge pressure of 0 Pa at both outlets (*left*), increasing to 25 Pa and then to 35 Pa at the branch 2 outlet. Note the relative reduction in magnitude of the TRWSS in the wide-angle daughter branch (*left to right*). **B:** Increasing gauge pressure at the branch 2 outlet results in flow velocity reduction in branch 2 and increase in branch 1 (*left panel*), with corresponding concordant changes in longitudinal wall shear stress (WSS) (*middle panel*). In contrast, the TRWSS remains grossly unchanged in the narrow-angle (Φ_1 = 30°) daughter vessel branch despite increasing flow velocity and longitudinal WSS in branch 1; wide-angle branch 2 exhibits significant decreases in TRWSS with decreasing flow as gauge pressure is increased to 35 Pa (*right panel*). Figure is available in color online only.

Brought to you by Tufts University | Unauthenticated | Downloaded 11/04/25 02:24 PM UTC

infinite possible morphological combinations, we chose to simulate changes in vessel resistance by applying nonzero outlet gauge pressure, which showed that TRWSS is sensitive to conditions impacting downstream vessel resistance, not only changes in radius but also potentially high branch curvature and high daughter-parent vessel inclination angle.[7] While all of these conditions need to be explored in future studies, the fact remains that aneurysmal bifurcations were statistically associated with higher TRWSS and TRWSSG. We hope that future studies will explore relevant morphological variations of parametric models, including daughter vessels of different diameters, variations in inclination angle,[7] and the behavior of TRWSS in the presence of aneurysm.

We have shown previously that wider bifurcations sustain longitudinal hemodynamic stresses (low WSS, high WSS peaks, positive WSSG) distally from the apex[8,11] and potentially outside the medial pad protection.[10,22] The newly identified transverse component, TRWSS, adds a new dimension to the hemodynamic insult at the apical area by quantifying significant forces acting in multiple directions in close proximity of the apex, distally deep into the daughter vessels. Future studies will evaluate the role of this transverse component on aneurysm progression after endovascular treatment such as coiling or endovascular flow diversion without alteration of the underlying bifurcation geometry. We have previously shown that stenting across bifurcations leads to angle decrease, vessel straightening, and hemodynamic alterations at the apex, and more recently flow diversion was shown to decrease curvature in the internal carotid artery.[23] Specifically, work from our laboratory has shown stent-induced angular remodeling with return to a narrow angle after both single- and Y-stent coil embolization.[24,25] Such beneficial remodeling would act to decrease the deleterious aneurysmogenic TRWSS described in this paper and may contribute to the lower recurrence of stent-coiled aneurysms described in the literature.[26]

Study Limitations

The findings of this study also bring to light the question of causation. This study is retrospective in nature and includes only a small number of patient-derived models. Parametric modeling was performed by angle variations only, while maintaining constant vessel caliber. It is thus challenging to determine if high TRWSS is a causal factor for aneurysm formation or if high TRWSS is a postorigination phenomenon. The conclusions of this study require further evaluations of TRWSS in larger studies to determine the possible implications for aneurysm analysis.

Conclusions

The current study characterized a clear association between wide bifurcation angle and significant vortex formation from flow recirculation and an associated transverse rotational positive WSS and shear gradient conditions. This TRWSS adds a new hemodynamic insult beginning near the apex but extending deep into downstream daughter vessels, away from the protection of the intimal pad in wide-angle bifurcations. The resulting deleterious hemodynamic microenvironment may trigger destructive remodeling previously associated with coexisting positive WSS and positive WSSG, contributing to aneurysm development and progression.

References

1. Sforza DM, Putman CM, Cebral JR. Hemodynamics of cerebral aneurysms. *Annu Rev Fluid Mech*. 2009;41(1):91-107.
2. Nixon AM, Gunel M, Sumpio BE. The critical role of hemodynamics in the development of cerebral vascular disease. *J Neurosurg*. 2010;112(6):1240-1253.
3. Meng H, Wang Z, Hoi Y, Gao L, Metaxa E, Swartz DD, Kolega J. Complex hemodynamics at the apex of an arterial bifurcation induces vascular remodeling resembling cerebral aneurysm initiation. *Stroke*. 2007;38(6):1924-1931.
4. Metaxa E, Tremmel M, Natarajan SK, Xiang J, Paluch RA, Mandelbaum M, et al. Characterization of critical hemodynamics contributing to aneurysmal remodeling at the basilar terminus in a rabbit model. *Stroke*. 2010;41(8):1774-1782.
5. Wang Z, Kolega J, Hoi Y, Gao L, Swartz DD, Levy EI, et al. Molecular alterations associated with aneurysmal remodeling are localized in the high hemodynamic stress region of a created carotid bifurcation. *Neurosurgery*. 2009;65(1):169-178.
6. Nagel T, Resnick N, Dewey CF Jr, Gimbrone MA Jr. Vascular endothelial cells respond to spatial gradients in fluid shear stress by enhanced activation of transcription factors. *Arterioscler Thromb Vasc Biol*. 1999;19(8):1825-1834.
7. Baharoglu MI, Lauric A, Safain MG, Hippelheuser J, Wu C, Malek AM. Widening and high inclination of the middle cerebral artery bifurcation are associated with presence of aneurysms. *Stroke*. 2014;45(9):2649-2655.
8. Tütüncü F, Schimansky S, Baharoglu MI, Gao B, Calnan D, Hippelheuser J, et al. Widening of the basilar bifurcation angle: association with presence of intracranial aneurysm, age, and female sex. *J Neurosurg*. 2014;121(6):1401-1410.
9. Canham PB, Finlay HM. Morphometry of medial gaps of human brain artery branches. *Stroke*. 2004;35(5):1153-1157.
10. Finlay HM, Whittaker P, Canham PB. Collagen organization in the branching region of human brain arteries. *Stroke*. 1998;29(8):1595-1601.
11. Lauric A, Hippelheuser JE, Malek AM. Induction of aneurysmogenic high positive wall shear stress gradient by wide angle at cerebral bifurcations, independent of flow rate. *J Neurosurg*. 2018;131(2):442-452.
12. Baharoglu MI, Lauric A, Wu C, Hippelheuser J, Malek AM. Deviation from optimal vascular caliber control at middle cerebral artery bifurcations harboring aneurysms. *J Biomech*. 2014;47(13):3318-3324.
13. Rossitti S, Löfgren J. Vascular dimensions of the cerebral arteries follow the principle of minimum work. *Stroke*. 1993;24(3):371-377.
14. Schirmer CM, Malek AM. Wall shear stress gradient analysis within an idealized stenosis using non-Newtonian flow. *Neurosurgery*. 2007;61(4):853-864.
15. Malek AM, Alper SL, Izumo S. Hemodynamic shear stress and its role in atherosclerosis. *JAMA*. 1999;282(21):2035-2042.
16. Bowker TJ, Watton PN, Summers PE, Byrne JV, Ventikos Y. Rest versus exercise hemodynamics for middle cerebral artery aneurysms: a computational study. *AJNR Am J Neuroradiol*. 2010;31(2):317-323.
17. Antiga L, Piccinelli M, Botti L, Ene-Iordache B, Remuzzi A, Steinman DA. An image-based modeling framework for patient-specific computational hemodynamics. *Med Biol Eng Comput*. 2008;46(11):1097-1112.
18. Alnaes MS, Isaksen J, Mardal KA, Romner B, Morgan MK,

Brought to you by Tufts University | Unauthenticated | Downloaded 11/04/25 02:24 PM UTC

Ingebrigtsen T. Computation of hemodynamics in the circle of Willis. *Stroke*. 2007;38(9):2500-2505.
19. Zamir M, Wrigley SM, Langille BL. Arterial bifurcations in the cardiovascular system of a rat. *J Gen Physiol*. 1983;81(3):325-335.
20. Ingebrigtsen T, Morgan MK, Faulder K, Ingebrigtsen L, Sparr T, Schirmer H. Bifurcation geometry and the presence of cerebral artery aneurysms. *J Neurosurg*. 2004;101(1):108-113.
21. Kasuya H, Shimizu T, Nakaya K, Sasahara A, Hori T, Takakura K. Angles between A1 and A2 segments of the anterior cerebral artery visualized by three-dimensional computed tomographic angiography and association of anterior communicating artery aneurysms. *Neurosurgery*. 1999;45(1):89-94.
22. Rowe AJ, Finlay HM, Canham PB. Collagen biomechanics in cerebral arteries and bifurcations assessed by polarizing microscopy. *J Vasc Res*. 2003;40(4):406-415.
23. Awad AW, Kilburg C, Karsy M, Couldwell WT, Taussky P. Change in the angle of the anterior genu is associated with occlusion rate after Pipeline flow diversion. *J Neurosurg*. 2019;132(1):109-113.
24. Gao B, Baharoglu MI, Cohen AD, Malek AM. Stent-assisted coiling of intracranial bifurcation aneurysms leads to immediate and delayed intracranial vascular angle remodeling. *AJNR Am J Neuroradiol*. 2012;33(4):649-654.
25. Gao B, Baharoglu MI, Cohen AD, Malek AM. Y-stent coiling of basilar bifurcation aneurysms induces a dynamic angular vascular remodeling with alteration of the apical wall shear stress pattern. *Neurosurgery*. 2013;72(4):617-629.
26. Chalouhi N, Jabbour P, Singhal S, Drueding R, Starke RM, Dalyai RT, et al. Stent-assisted coiling of intracranial aneurysms: predictors of complications, recanalization, and outcome in 508 cases. *Stroke*. 2013;44(5):1348-1353.

Disclosures

The authors report no conflict of interest concerning the materials or methods used in this study or the findings specified in this paper.

Author Contributions

Conception and design: Malek. Acquisition of data: Malek, Hippelheuser. Analysis and interpretation of data: all authors. Drafting the article: Lauric. Critically revising the article: all authors. Approved the final version of the manuscript on behalf of all authors: Malek. Statistical analysis: Hippelheuser, Lauric. Study supervision: Malek.

Supplemental Information

Videos

Video 1. https://vimeo.com/569335148.
Video 2. https://vimeo.com/569336784.

Correspondence

Adel M. Malek: Tufts Medical Center, Boston, MA. amalek@tuftsmedicalcenter.org.

Brought to you by Tufts University | Unauthenticated | Downloaded 11/04/25 02:24 PM UTC